ISSN 0021-3640, JETP Letters, 2016, Vol. 103, No. 7, pp. 443–448. © Pleiades Publishing, Inc., 2016.

OPTICS AND LASER PHYSICS

Spin-Dependent Transverse Force on a Vortex Light Beam in an Inhomogeneous Medium[1]

N. I. Petrov

Scientific and Technological Centre of Unique Instrumentation, Russian Academy of Sciences, Moscow, 117342 Russia

e-mail: petrovni@mail.ru

Received November 10, 2015; in final form, February 19, 2016

Spin-dependent effects on vortex light beams propagating in an inhomogeneous medium are demonstrated by solving the full three-component field Maxwell equations using the perturbation analysis. It is found that the hybrid Laguerre–Gauss modes with polarization-orbital angular momentum (OAM) entanglement are the vector solutions of the Maxwell equations in a graded-index medium. Focusing of linearly and circularly polarized vortex light beams in a cylindrical graded-index medium is investigated. It is shown that the vortex light beam undergoes an additional transverse force acting differently on circular polarized beams with opposite handedness. The wave shape variation with distance taking into account the spin–orbit and nonparaxial effects is analyzed. Effect of long-term periodical revival of wave packets due to mode interference in a graded-index cylindrical optical waveguide is demonstrated.

DOI: 10.1134/S0021364016070122

1. INTRODUCTION

In a scalar approximation, the light beam propagating in an inhomogeneous medium is governed by diffractive and refractive forces. When a vector wave field is considered, the influence of additional effective forces associated with the polarization (spin angular momentum, SAM) and orbital angular momentum (OAM) should be included. It is well established that the polarization vector of linearly polarized optical beams propagating over a spiral trajectory undergoes the Rytov rotation [1, 2]. It is also of interest to consider the inverse effect, i.e., the influence of polarization on the trajectory and the width of a radiation beam. Recently, the influence of polarization on the trajectory of a light beam propagating in an inhomogeneous medium (the optical Magnus effect or spin Hall effect) has been predicted and studied [3]. The spin Hall effect (SHE) was predicted by Dyakonov and Perel' [4] in solid state physics, it originates from the coupling of the charge and spin currents due to spin–orbit interaction (SOI). Note that there are analogues between the SOI of light and the spin–orbit interaction of electrons in solids [5]. In [6] spin transverse force was proposed for electron spin moving in an electric field in non-relativistic quantum mechanical limit of Dirac equation or in semiconductor with spin–orbit coupling.

It is well known that, when a light beam is reflected from an interface, the longitudinal shift of the gravity center of the beam is different for *s*- and *p*-polarized beams [7], while the transverse shift has reverse signs in the case of right- and left-hand circularly polarized radiation [8]. Lateral and angular shifts for strongly focused azimuthally and radially polarized beams at a dielectric interface were shown in [9]. As demonstrated in [3, 10], these Goos–Hanchen effects can also be observed in optical waveguides. In [11] it was experimentally demonstrated that the rotation angle of the speckle pattern depends on the angle at which a circularly polarized light beam is coupled into a fiber. It was shown in [12] that spin–orbit interaction causes asymmetry effect for depolarization of the right- and left-handed circularly polarized light propagating in a graded-index fiber. The depolarization is stronger if the spirality of the rays' trajectory and photons have the same signs and it is less if they are not the same. The spin-dependent relative shift between right- and left-hand circularly polarized light beams propagating along a helical trajectory in a graded-index fiber was shown in [13]. It was shown in [14] that the propagation of the rays with right- and left-hand circularly polarization along different trajectories is due to the anisotropy of the Berry's phase. In [15], this effect was observed experimentally for a laser beam propagating in the glass cylinder along the smooth helical trajectory. This shift can be regarded as a manifestation of the optical Magnus effect [3] and the optical spin-Hall

[1] The article is published in the original. See the supplemental material for this paper at www.jetpletters.ac.ru.

effect [16, 17] which arises due to a spin–orbit coupling.

In this paper the influence of polarization (spin) and OAM on a vortex light beam propagating through the cylindrically symmetric waveguide with a gradient profile of the refractive index is investigated by solving the full three-component field Maxwell equations.

2. MODEL

The Maxwell equations for the electric field $\mathbf{E}\exp(-ivt)$ in a general inhomogeneous medium with the dielectric constant $\varepsilon(x, y)$ reduce to [18]:

$$\begin{aligned}(\nabla_\perp^2 + k^2n^2)\mathbf{e}_\perp - i\beta\nabla_\perp e_z - \nabla_\perp\nabla_\perp\mathbf{e}_\perp = \beta^2\mathbf{e}_\perp,\\ (\nabla_\perp^2 + k^2n^2)e_z + i\beta\mathbf{e}_\perp\nabla_\perp \ln n^2 = \beta^2 e_z,\end{aligned} \quad (1)$$

where $k = 2\pi/\lambda$ is the wavenumber and $n^2(x, y)$ is the dielectric permittivity of the medium, β is the propagation constant.

It is assumed that the dependence on time and z is $\exp[-i(\nu t - \beta z)]$. Usually the vector wave equation $\nabla^2\mathbf{E} + k^2n^2\mathbf{E} + \nabla(\mathbf{E}\nabla\ln n^2) = 0$ is considered, which is followed from Eqs. (1) by substituting $e_z = (i/\beta)(\nabla_\perp\mathbf{e}_\perp + \mathbf{e}_\perp\nabla_\perp\ln n^2)$ coming from the condition $\mathrm{div}(n^2\mathbf{E})$ into the first equation. Here, we use the system of Eqs. (1). Note, that this system includes the small component e_z analogically to Dirac equation for the quasi-relativistic wavefunction of an electron $\begin{pmatrix}\varphi\\ \chi\end{pmatrix}$, where $\chi \ll \varphi$ [19].

Rewrite the system (1) in the form

$$\left(\nabla_\perp^2 + k^2n^2 + W_0 + \frac{1}{4}P^2\right)\mathbf{E} = \left(\beta - \frac{1}{2}P\right)^2\mathbf{E}, \quad (2)$$

where $\mathbf{E} = \begin{pmatrix}e_x\\ e_y\\ e_z\end{pmatrix}$, $W_0 = \begin{pmatrix}-\frac{\partial^2}{\partial x^2} & -\frac{\partial^2}{\partial x\partial y} & 0\\ -\frac{\partial^2}{\partial y\partial x} & -\frac{\partial^2}{\partial y^2} & 0\\ 0 & 0 & \end{pmatrix}$, $P = \begin{pmatrix}0 & 0 & -i\frac{\partial}{\partial x}\\ 0 & 0 & -i\frac{\partial}{\partial y}\\ \frac{i}{n^2}\frac{\partial n^2}{\partial x} & \frac{i}{n^2}\frac{\partial n^2}{\partial y} & 0\end{pmatrix}$. By formally taking the square root of both sides, we have an equation which is equivalent to the stationary Schrödinger equation for the reduced field $\mathbf{\Psi}(x, y)$:

$$\hat{H}\mathbf{\Psi} = \varepsilon\mathbf{\Psi}, \quad (3)$$

where $\varepsilon = \delta\beta = kn_0 - \beta$ and $\mathbf{\Psi}(x, y)$ are the eigenvalue and eigenfunction of the Hamiltonian, respectively, $n_0 = n(0, 0)$,

$$\hat{H} = \hat{H}^{(0)} + \hat{H}^{(1)} + \cdots, \quad (4)$$

$$\hat{H}^{(0)} = \mathscr{H}_0 - \Re, \quad \mathscr{H}_0 = \hat{H}_0 - \frac{1}{2k^2n_0^2}\hat{W}_0,$$

$$\hat{H}_0 = -\frac{1}{2k^2n_0^2}\nabla_\perp^2 + \frac{1}{2n_0^2}(n_0^2 - n^2),$$

$\hat{H}^{(1)}$ is the nonparaxial correction to the operator of paraxial propagation, which has the form

$$\hat{H}^{(1)} = \frac{1}{2}\mathscr{H}_0^2 - \frac{1}{2}\Re^2, \quad \hat{\Re} = \frac{P}{2kn_0}.$$

The procedure contains an expansion in terms of a small parameter $\eta = 1/kw_0$, where w_0 is the beam spot size. Below the effects of the order of η^2 are considered.

Note that the Hamiltonian (4) can also be easily expressed by means of spherical tensor operators $\hat{\tau}_{KQ}$ [18]. It was shown in [20] that vector and tensor operators completely describe the three-dimensional polarization. The mean values $t_{1Q} = \langle\hat{\tau}_{1Q}\rangle$ and $t_{2Q} = \langle\hat{\tau}_{2Q}\rangle$ describe the vector (rank 1) and tensor (rank 2) polarizations, respectively.

Consider a rotationally symmetric cylindrical waveguide with a parabolic distribution of the refractive index:

$$n^2(r) = n_0^2 - \omega^2r^2, \quad (5)$$

where n_0 is the refractive index on the waveguide axis, ω is the gradient parameter, $r = (x^2 + y^2)^{1/2}$.

The graded-index potential is chosen because in this case the 3D polarization evolution problem can be solved analytically.

The Hamiltonian $\hat{H}$ may be rewritten in terms of annihilation and creation operators in cylindrical coordinates [18], i.e., $\hat{H}_0 = (\omega/kn_0^2)(\hat{A}_1^+\hat{A}_1 + \hat{A}_2^+\hat{A}_2 + 1)\hat{I}$.

The representation of the Hamiltonian via the operators will allow us to calculate the matrix elements analytically. Indeed, calculating the integrals $\langle v', l'|\hat{A}_{1,2}|v, l\rangle = \int\int d\varphi r dr\psi^*_{v'l'}\hat{A}_{1,2}\psi_{vl}$ we obtain the following relations defining the action of operators on modal solutions:

$$\begin{aligned}\hat{A}_1|v, l\rangle &= -\sqrt{\frac{v-l}{2}}|v-1, l+1\rangle,\\ \hat{A}_1^+|v, l\rangle &= -\sqrt{\frac{v-l}{2}+1}|v+1, l-1\rangle,\\ \hat{A}_2|v, l\rangle &= \sqrt{\frac{v+l}{2}}|v-1, l-1\rangle,\\ \hat{A}_2^+|v, l\rangle &= \sqrt{\frac{v+l}{2}+1}|v+1, l+1\rangle.\end{aligned} \quad (6)$$

These important relationships allow us to find the matrix elements with the help of pure algebraic procedure without the calculations of integrals. The solution of the unperturbed equation is described by radially symmetric Laguerre–Gauss functions $\psi_{vl}(r, \varphi) = |v, l\rangle$:

$$\psi_{vl}(r,\varphi) = \left(\frac{k\omega}{\pi}\right)^{1/2}\left[\frac{p!}{(p+l)!}\right]^{1/2}(k\omega r^2)^{l/2} \times\exp\left(-\frac{k\omega r^2}{2}\right)L_p^l(k\omega r^2)\exp(il\varphi), \quad (7)$$

where $v = 2p + l$ is the principal quantum number; p and l are the radial and azimuthal indices, respectively; and $l = v, v-2, v-4, \ldots, 1$ or 0, $\omega = 2/(kw_0^2)$, w_0 is the radius of the fundamental mode.

The numbers v and l express the eigenvalues of the unperturbed Hamiltonian $\hat{H}_0|v,l\rangle = (\omega/kn_0^2)(v+1)|v,l\rangle$, and eigenvalues $L = l/k$ of the angular momentum operator $\hat{L}_z|v,l\rangle = (l/k)|v,l\rangle$.

There is no mode conversion at propagation if the incident beam is expressed by the hybrid wavefunctions consisting of transverse and longitudinal components:

$$\hat{H}^{(0)} = \begin{vmatrix} |vl\rangle \\ i\sigma|vl\rangle \\ e_z \end{vmatrix} = \frac{\omega}{kn_0^2}(v+1)\begin{vmatrix} |vl\rangle \\ i\sigma|vl\rangle \\ e_z \end{vmatrix}, \quad (8)$$

where $\sigma = +1$ and -1 correspond to right-handed and left-handed circularly polarized beams, respectively, and $\sigma = 0$ corresponds to the linear polarization.

Note that the hybrid wavefunction (8) cannot be factorized into the product of spin and orbital parts since the mixing of OAM and SAM exists. Thus, the modal solutions of the Maxwell equations in a GRIN media are the hybrid vector Laguerre–Gauss modes with the spin–orbit entanglement. The longitudinal field component can be expressed through the transverse field components, i.e., $|e_z\rangle = (i/kn_0)\nabla_\perp \mathbf{e}_\perp$.

The propagation constant correct to first-order non-paraxial term $\hat{H}^{(1)}$ of the Hamiltonian is given by [21]:

$$\beta_{vl\sigma} = kn_0\left\{1 - \eta(v+1) - \frac{\eta^2}{32} \times[1\,1(v+1)^2 - (l+\sigma)^2 - 2(l+\sigma)\sigma]\right\}, \quad (9)$$

where $\eta = \omega/kn_0^2$.

3. SIMULATION RESULTS

Consider the incident vector vortex beams with right and left circular polarizations, respectively:

$$\langle\mathbf{\Psi}_0^+| = (\langle vl|, -i\langle vl|, e_z), \quad \langle\mathbf{\Psi}_0^-| = (\langle vl|, i\langle vl|, e_z), \quad (10)$$

where $|vl\rangle = \psi_{vl}(r, \varphi) = (k\omega'/\pi)^{1/2}[p!/(p+l)!]^{1/2}(k\omega' r^2)^{l/2} \times \exp(-k\omega' r^2/2)L_p^l(k\omega' r^2)\exp(il\varphi)$, $\omega' = 2/(ka_0^2)$, a_0 is the radius of a beam, which is different from the radius of the fundamental mode of the medium $w_0 = \sqrt{2/(k\omega)}$).

The trajectory and width of the radiation beam can be expressed in terms of the relevant matrix elements:

$$\Delta r^2 = \frac{\langle\psi|\hat{U}^+ r^2\hat{U}|\psi\rangle}{\langle\psi|\hat{U}^+\hat{U}|\psi\rangle} - \frac{\langle\psi|\hat{U}^+ r\hat{U}|\psi\rangle^2}{\langle\psi|\hat{U}^+\hat{U}|\psi\rangle^2}, \quad (11)$$

where $\hat{U} = \exp(-ikn_0\hat{H}z)$.

Calculating the matrix elements in (11) within the accuracy of the small parameter $(\omega/k)^2$ we obtain the following expression for the beam radius:

$$\langle\Delta r^2\rangle \cong \frac{v+1}{2k\omega}\left[1 - \frac{j\sigma}{4}(\omega z)^2 + \frac{1}{4}(1+2l\sigma)(\omega z)^2\right], \quad (12)$$

where $j = l + \sigma$ is the total angular momentum, $\omega' = \omega$.

It is followed from (12) that the beam spot radius of the circularly polarized light does not change with distance if the azimuthal l index is zero. It is seen that beams with antiparallel OAM and SAM can be focused into tighter spots than those for which these angular momentum are parallel. Difference (asymmetry) between the spot sizes of the beams with right- and left-circularly polarizations is given by

$$D = \langle\Delta r^2\rangle^+ - \langle\Delta r^2\rangle^- = \frac{(v+l)l}{4k\omega}(\omega z)^2 > 0. \quad (13)$$

It is seen that the difference D increases with l. Similar result was obtained from the uncertainty-type relations between focal spot size and angular spread [22]. Although the obtained solutions have obvious demonstration of the average beam radius evolution in a graded-index fiber, the derivation of the expression for long distances requires cumbersome calculations. A more efficient method is the use of modal expansion of the incident beam in order to take into account the accumulative effects with distance. As was shown before (Eq. (8)), the hybrid vortex Laguerre–Gauss functions with polarization-orbital angular momentum entanglement are the modal solutions.

The arbitrary incident beam may be expanded into modal solutions, so the evolution of a beam in the medium (5) can be represented as

$$\Psi(r,\varphi,z) = \sum_{vl\sigma} a_{vl\sigma} \left| \begin{matrix} |vl\rangle \\ i\sigma|vl\rangle \\ (i/kn_0)\nabla_\perp(x+i\sigma y)|vl\rangle \end{matrix} \right\rangle \exp(i\beta_{vl\sigma}z), \quad (14)$$

where $a_{vl\sigma}$ are the coupling coefficients.

Below only the propagating modes are considered, the evanescent waves do not reach the far-field zone.

If the incident beam is described by the Laguerre–Gauss function $\Psi^*_{v'l'\sigma} = (1/\sqrt{2})\langle\langle v'l'|, -i\sigma\langle v'l'|, e_z^*|$, the coupling coefficients $a_{vl\sigma}$ can be calculated analytically:

$$\langle vl\sigma|v'l\sigma\rangle = \left(\frac{2\sqrt{\omega\omega'}}{\omega+\omega'}\right)^{l+1} \times \left(\frac{\omega'-\omega}{\omega'+\omega}\right)^{p-p'} \left(\frac{p'!(p+l)!}{(p'+l)!p!}\right)^{1/2} P_{p'}^{[p-p',l]}(z), \quad (15)$$

where $z = 1 - 2((\omega'-\omega)/(\omega'+\omega))^2$, $P_{p'}^{[p-p',l]}(z)$ are the Jacobi polynomials, $\omega' = 2/ka_0^2$, $\omega = 2/kw_0^2$. The wave shape variations with distance are determined by the functions $I_\perp(r,\varphi,z) = |\psi(r,\varphi,z)|^2$ and $I_z(r,\varphi,z) = |e_z(r,\varphi,z|^2$. Figure 1 shows the intensity profiles of the linearly polarized beams with different OAM in the focal plane. The medium (5) with the gradient parameter $\omega = 7 \times 10^{-3}$ μm^{-1} and the refractive index $n_0 = 1.5$ is considered. These parameters are reasonable for conventional graded-index optical fibers. Here and below, the beams with wavelength $\lambda = 0.63$ μm are considered. The numerical aperture is determined by $NA = a\omega = n_0\sqrt{2\Delta}$, where a is the radius of the waveguide and $\Delta \approx [n_0 - n(a)]/n_0$. The initial beam width or the full width at half maximum (FWHM) is $a_0 = 45$ μm. It is seen that the intensity distributions depend on the SAM and OAM of the incident beam. For $l = 0$ the focused spot in the longitudinal field component is splitting into two equal parts (Fig. 1b). There is an asymmetry between the longitudinal field component intensity distributions for the incident beams with opposite OAM (Figs. 1f and 1h). Note, that there is no such asymmetry for the transverse field components.

It is followed from the simulations (see Supplemental Material [23]) that the beams with antiparallel OAM and SAM can achieve tighter focal spots than those for which the signs of the helicity and the orbital angular momentum are the same. High efficiency transfer of a strongly focused spot through optical waveguide over large distances with a period of revival is shown. Note that the long-term revivals of the focused spots have very close analogue with the long-term evolution of quantum wave packets in systems executing regular periodic motion in the classical limit [24, 25]. The effect of long-term revival of wave packets due to mode interference at nonparaxial propagation in a planar waveguide was considered in [26]. Here, this phenomenon is demonstrated in cylindrically symmetric waveguide, where the long-term revival occurs due to spin–orbit and nonparaxial effects.

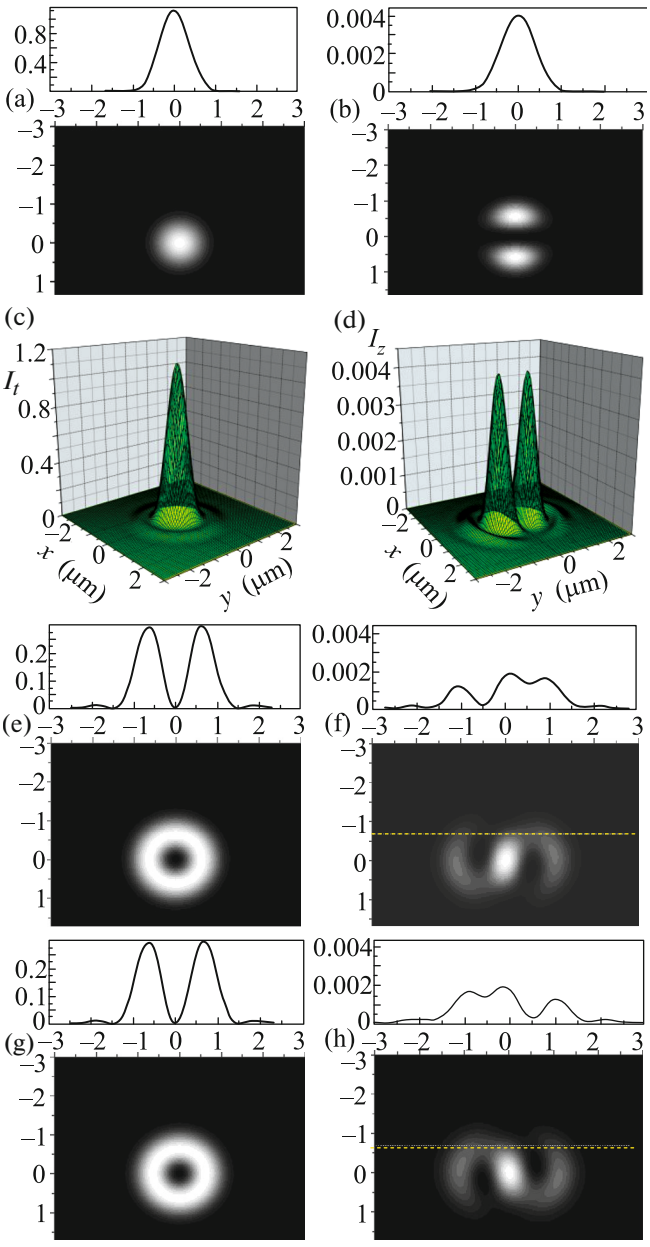

Fig. 1. (Color online) Intensity profiles of (left column) the transverse electric field component and (right column) the longitudinal electric field component for the linearly polarized incident beam in the focal plane $z_f = 331$ μm: (a, b) $l = 0$; (c, d) $l = 0$, 3D intensity patterns; (e, f) $l = 1$; (g, h) $l = -1$.

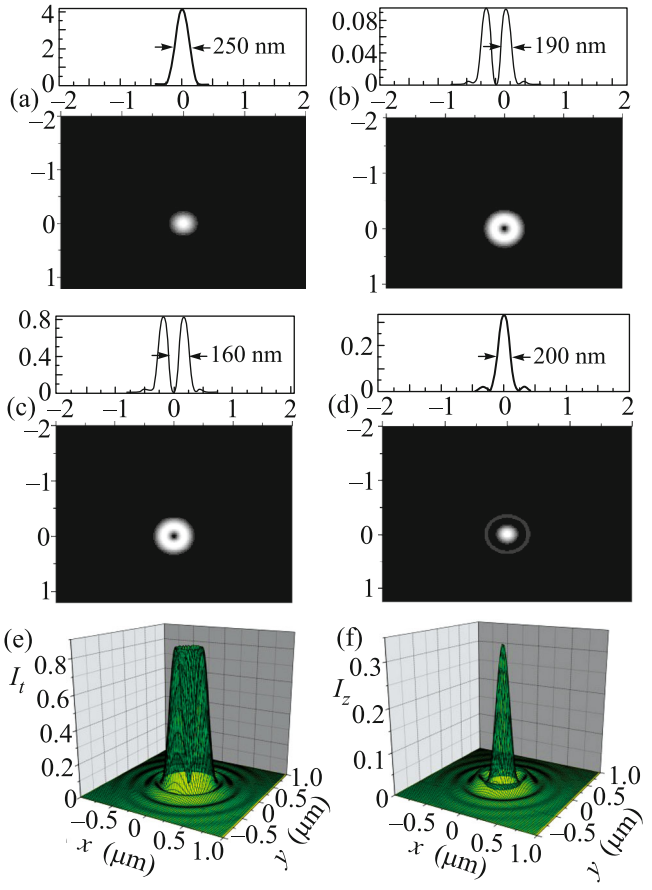

Fig. 2. (Color online) Long-term transfer of a subwavelength focused spot in a waveguide with $\omega = 0.1\ \mu m^{-1}$. Intensity profiles of (left column) the transverse electric field component and (right column) the longitudinal electric field component in the focal plane $z = 205$ mm: (a, b) $l = 0$, $\sigma = 1$; (c–f) $l = 1$, $\sigma = -1$; (e, f) 3D intensity patterns of the intensity profiles (c) and (d), respectively.

Consider the propagation of a strongly focused Gaussian beam in a medium (5). Note that only the propagating modes reach the far-field zone. For the beam with $a_0 \geqslant \lambda/(2NA)$ all incident power is in the propagating modes and the periodical revivals of the initial field intensity distribution occur at extremely long distances. In Figs. 2a and 2b the electric field intensity distributions in a transverse plane $z =$ 205 mm in a waveguide with $NA = 1.0$ are shown for the incident beam with a FWHM of 176 nm. The power contained in the propagating modes amounts to $P_\perp \approx 86\%$ and $P_z \approx 6.6\%$ of the total beam power if $l = 0$ and $P_\perp \approx 60\%$ and $P_z \approx 7.3\%$, if $l = 1$. Note, that the spots and doughnut rings with a FWHM smaller than $\lambda/(2NA)$ can be transferred with the help of propagating modes (Fig. 2). It is seen that the tighter focal spots and thinner doughnut rings can be transferred into long distances if the vortex incident beam is considered. It is followed from the calculations that the periodical revivals of the initial field intensity distribution occur at extremely long distances and the high efficiency transfer of the subwavelength spot through optical waveguide over large distances takes place with a period of revival.

4. CONCLUSIONS

In conclusion, propagation of vector vortex beams in an inhomogeneous medium is analyzed by solving three-component field Maxwell equations. The polarization-dependent properties of the electric field intensity profiles in the focal plane are examined for the beams with OAM and SAM. The asymmetry caused by the spin–orbit and tensor interactions of light is demonstrated. It is shown that the beams with antiparallel OAM and SAM can be focused into tighter spots than those for which these angular momenta are parallel. The fundamental effect of collapse and revival of wave packets at the propagation in rotationally symmetric waveguide is examined. The long-term periodical revival of a focused incident beam profile taking into account the spin–orbit and nonparaxial effects is demonstrated. Due to this effect the remote subwavelength focusing of a light beam in an optical fiber can be achieved without the use of the evanescent waves. Vector modal solutions exhibiting entanglement between spin (polarization) and OAM (wavefront vorticity) may be useful for classical implementations of quantum communication and computational tasks [27].

REFERENCES

1. S. M. Rytov, Dokl. Akad. Nauk USSR **18**, 263 (1938).
2. V. V. Vladimirsky, Dokl. Akad. Nauk USSR **31**, 222 (1941).
3. B. Ya. Zel'dovich and V. S. Liberman, Sov. J. Quantum Electron. **20**, 427 (1990); V. S. Liberman and B. Y. Zel'dovich, Phys. Rev. A **46**, 5199 (1992); A. V. Dugin, B. Ya. Zeldovich, N. D. Kundikova, and V. S. Liberman, JETP Lett. **53**, 186 (1991).
4. M. I. Dyakonov and V. I. Perel, JETP Lett. **13**, 467 (1971), Phys. Lett. A **35**, 459 (1971).
5. E. I. Rashba, Sov. Phys. Solid State **2**, 1109 (1960); Phys. E **34**, 31 (2006).
6. S. Q. Shen, Phys. Rev. Lett. **95**, 187203 (2005).
7. F. Goos and H. Hanchen, Ann. Phys. Lpz. **436**, 333 (1947).
8. C. Imbert, Phys. Rev. D **5**, 787 (1972).
9. N. I. Petrov, Opt. Lett. **29**, 421 (2004), J. Mod. Opt. **52**, 1545 (2005).
10. N. I. Petrov, J. Opt. **15**, 014011 (2013).
11. B. Y. Zel'dovich, I. V. Kitaevskaya, and I. D. Kundikova, Quant. Electron. **23**, 89 (1996).
12. N. I. Petrov, J. Mod. Opt. **43**, 2239 (1996), Phys. Lett. A **234**, 239 (1997); J. Exp. Theor. Phys. **85**, 1085 (1997).
13. N. I. Petrov, Laser Phys. **10**, 619 (2000).

14. K. Yu. Bliokh and Yu. P. Bliokh, JETP Lett. **79**, 519 (2004); K. Y. Bliokh, Phys. Rev. Lett. **97**, 043901 (2006).
15. K. Y. Bliokh, A. Niv, V. Kleiner, and E. Hasman, Nature Photon. **2**, 748 (2008).
16. M. Onoda, S. Murakami, and N. Nagaosa, Phys. Rev. Lett. **93**, 083901 (2004).
17. A. Kavokin, G. Malpuech, and M. Glazov, Phys. Rev. Lett. **95**, 136601 (2005).
18. N. I. Petrov, Phys. Rev. A **88**, 023815 (2013).
19. V. B. Berestetskii, E. M. Lifshitz, and L. P. Pitaevskii, *Course of Theoretical Physics*, Vol. 4: *Quantum Electrodynamics* (Nauka, Moscow, 1989; Pergamon, Oxford, 1982).
20. N. I. Petrov, Laser Phys. **18**, 522 (2008).
21. N. I. Petrov, Opt. Lett. **38**, 2020 (2013).
22. M. A. Alonso, J. Opt. **13**, 064016 (2011).
23. Supplementary Materials. www.jetpletters.ac.ru
24. I. S. Averbukh and N. F. Perelman, Sov. Phys. JETP **69**, 464 (1989).
25. R. Arvieu and P. Rozmej, Phys. Rev. A **50**, 4376 (1994).
26. N. I. Petrov, Phys. Rev. A **90**, 043814 (2014).
27. J. T. Barreiro, T. C. Wei, and P. G. Kwiat, Phys. Rev. Lett. **105**, 030407 (2010).